Communication

Variance-Based Sensitivity Analysis of Fitting Parameters to Impact on Cycling Durability of Polymer Electrolyte Fuel Cells

Victor A. Kovtunenko [1,2]

1   Institute for Mathematics and Scientific Computing, Karl-Franzens University of Graz, NAWI Graz, Heinrichstr. 36, 8010 Graz, Austria; victor.kovtunenko@uni-graz.at
2   Lavrentyev Institute of Hydrodynamics, Siberian Division of the Russian Academy of Sciences, 630090 Novosibirsk, Russia

Abstract: Degradation of a catalyst layer in polymer electrolyte membrane fuel cells is considered, which is caused by electrochemical reactions of the platinum ion dissolution and oxide coverage. An accelerated stress test is applied, where the electric potential cycling is given by a non-symmetric square profile. Computer simulations of the underlying one-dimensional Holby–Morgan model predict durability of the fuel cell operating. A sensitivity analysis based on the variance quantifies how loss of the platinum mass subjected to the degradation is impacted by the variation of fitting parameters in the model.

Keywords: polymer electrolyte fuel cell; catalyst degradation; platinum dissolution and oxidation; accelerated stress test; variance-based sensitivity analysis; Pearson correlation coefficient

MSC: 78A57; 80A30; 80A32; 35K57

1. Introduction

Polymer electrolyte fuel cells (PEMFC) convert the chemical energy stored in hydrogen to electricity directly by the electrochemical reaction. They operate under lower temperature and have high efficiency and flexibility important for application in portable power sources and electric vehicles. Degradation of expensive platinum catalysts used in commercial power devices is currently under study in various academic and industrial organizations, which aim to increase the durability of polymer electrolyte membrane (PEM) fuel cells (FC). For understanding electrochemical mechanisms that cause the platinum surface degradation, we refer to [1–6] for diffusive models of platinum (Pt) degradation in a PEM catalyst layer (CL). One can find the related electrochemical modeling for nonlinear diffusion equations in [7–9] and Butler–Volmer equations in [10], multi-phase media with interface reactions in [11–15], and mechanical degradation caused by cracks in [16].

Holby and Morgan [17] and further Li et al [18] suggested the platinum degradation model based on the platinum ion (Pt^{2+}) dissolution:

$$Pt_{(s)} \longleftrightarrow Pt^{2+}_{(aq)} + 2e^-, \tag{1}$$

and the platinum oxide (PtO) surface coverage:

$$Pt_{(s)} + H_2O_{(aq)} \longleftrightarrow PtO_{(s)} + 2H^+_{(aq)} + 2e^-. \tag{2}$$
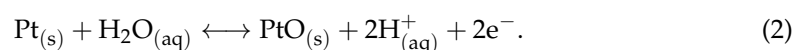
For chemical study of oxidation reaction in fuel cells, we refer to [19,20]. The one-dimensional model for (1) and (2) suggests the dissolution and diffusion into the ionomer membrane in one direction across CL, see sketch in Figure 1a.

Based on the one-dimensional Holby–Morgan model, in [21,22] we investigated durability of PEMFC in the accelerated stress test (AST) under cycling electric potentials with

various profiles: square used by Tennessee Tech University and the triangle developed by the U.S. Department of Energy and Nissan. Here, we study the non-symmetric square profile [23] suggested recently by the European consortium on fuel cells and hydrogen joint undertaking. In each cycle of the period of 40 s, the electric potential level switches between $V_{min} = 0.6$ (V) during 10 s and $V_{max} = 0.9$ (V) during 30 s, as shown in Figure 1b for five AST cycles within 200 s.
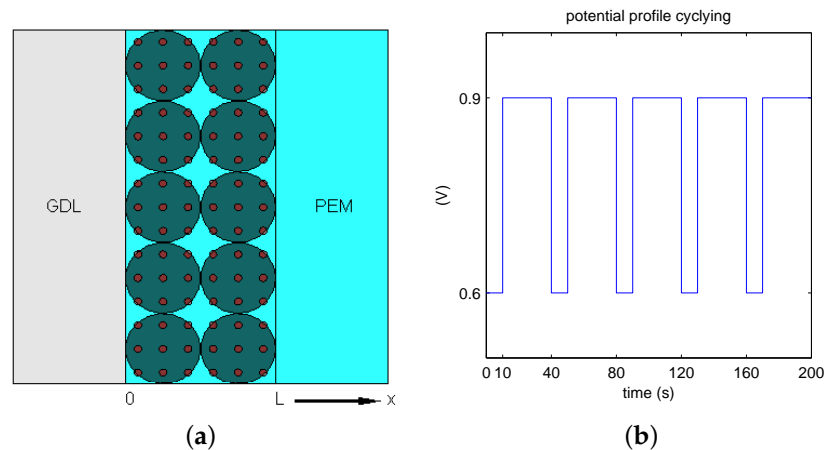
Figure 1. Sketch of the catalyst layer (**a**); five cycles of the electric potential cycling (**b**).

There are numerous studies on how operating conditions impact performance of PEMFC, e.g., we cite [24,25]. However, 30 input parameters in our degradation model include some fitting parameters characterizing the reference Pt ion concentration, bulk equilibrium voltage, and activation enthalpy for Pt dissolution and oxide formation. In the present study, we quantify the impact of the fitting parameters taken from the literature on the model output, which is the catalyst durability. The local sensitivity analysis is realized by a single parameter perturbation (the one-variable-at-a-time method). For the sensitivity index, the Pearson correlation coefficient (PCC) based on the covariance of input and output variables is argued in [26].

2. Materials and Methods

The physical parameters are taken from [22] and presented in Table 1 for Pt particles in CL, where the temperature T on the Kelvin scale corresponds to 80 °C.

Table 1. Parameters for cathode catalyst layer.

Symbol	Value	Units	Description
L	1×10^{-3}	cm	CL thickness
d_{Pt}	3×10^{-7}	cm	Pt particle diameter
V_{Pt}	1.5×10^{-20}	cm^3	Pt particle volume
ρ_{Pt}	21.45	g/cm^3	Pt particles density on carbon support
p_{Pt}	4×10^{-4}	g/cm^2	Pt particles loading on carbon support
ε_{Pt}	0.02		Pt volume fraction across CL
N_{Pt}	1.32×10^{18}	1/cm^3	Pt number concentration in CL
ε	0.2		volume fraction of ionomer increment in cathode
T	353.15	K	temperature

For platinum ion Pt^{2+} formation and diffusion, and for platinum oxide PtO formation, the parameters are presented in Table 2. The gas constant is $R = 8.31445985$ J/(mol×K), and the Faraday constant is $F = 96,485.3329$ C/mol.

Table 2. Parameters for Pt ion formation and diffusion and Pt oxide formation.

Symbol	Value	Units	Description
ν_1	1×10^4	Hz	dissolution attempt frequency
ν_2	8×10^5	Hz	backward dissolution rate factor
β_1	0.5		Butler–Volmer transfer coefficient for Pt dissolution
n	2		electrons transferred during Pt dissolution
Ω	9.09	cm^3/mol	molar volume of Pt
γ	2.4×10^{-4}	J/cm^2	Pt [1 1 1] surface tension
D_{Pt}	1×10^{-6}	cm^2/s	diffusion coefficient of Pt ion in the membrane
pH	0		potential of hydrogen ions (protons)
$\nu_1^\star$	1×10^4	Hz	forward Pt oxide formation rate constant
$\nu_2^\star$	2×10^{-2}	Hz	backward Pt oxide formation rate constant
Γ	2.2×10^{-9}	mol/cm^2	Pt surface site density
β_2	0.5		Butler–Volmer transfer coefficient for PtO formation
n_2	2		electrons transferred during Pt oxide formation
λ	2×10^4	J/mol	Pt oxide dependent kinetic barrier constant
ω	5×10^4	J/mol	Pt oxide-oxide interaction energy

In Table 3, we gather fitting parameters employed in the model.

Table 3. Fitting parameters.

Symbol	Value	Units	Description
U_{eq}	1.118	V	Pt dissolution bulk equilibrium voltage
c_{ref}	1	mol/cm^3	reference Pt ion concentration
$H_{1,fit}$	4×10^4	J/mol	Pt dissolution activation enthalpy
U_{fit}	0.8	V	Pt oxide formation bulk equilibrium voltage
$H_{2,fit}$	1.2×10^4	J/mol	partial molar oxide formation activation enthalpy

In Table 1 and the related discussion, the assumption of a perfectly deposited and regular catalyst layer is made; in Figure 1a, a plane surface without roughness and 100% coverage of the support is assumed. The realistic catalyst layer usually produced commercially is irregular and has a partial coverage at Pt particles by ionomer and carbon support. Details of the physical model are described in our previous publications [21,22]. Here, we formulate governing equations for numerical simulation.

For time $t \geq 0$, the electric potential difference $V(t)$ versus reference of 0 V is given by the square profile from Figure 1b. The space variable $x \in [0, L]$ is set across the CL, where the left end at $x = 0$ meets the gas diffusion layer (GDL), and the right end at $x = L$ confirms the interface with PEM, as sketched in Figure 1a. We look for the unknown Pt ion concentration $c(t, x) \geq 0$ (mol/cm^3), particle diameter $d(t, x) \geq 0$ (cm), and Pt oxide coverage ratio $\theta(t, x) \in [0, 1]$ satisfying

$$\frac{\partial c}{\partial t} - \sqrt{\varepsilon} D_{Pt} \frac{\partial^2 c}{\partial x^2} = B_3 d^2 r_{\text{dissol}}(c, d, \theta, V) \quad \text{for } t > 0, x \in (0, L), \tag{3}$$

where the notation $B_3 = \pi N_{Pt}/(2\varepsilon)$ (1/cm^3), and

$$\frac{\partial d}{\partial t} = -\Omega\, r_{\text{dissol}}(c, d, \theta, V) \quad \text{for } t > 0, x \in (0, L), \tag{4}$$

$$\frac{\partial \theta}{\partial t} + \frac{2\theta}{d} \frac{\partial d}{\partial t} = \frac{1}{\Gamma} r_{\text{oxide}}(\theta, V) \quad \text{for } t > 0, x \in (0, L). \tag{5}$$

For physical consistency, the Pt ion concentration and the particle diameter should be positive, and the Pt oxide coverage ratio lies between 0 and 1. The reaction–diffusion Equations (3)–(5) are endowed with the initial condition:

$$c = 0, \quad d = d_{\text{Pt}}, \quad \theta = 0 \quad \text{as } t = 0, x \in [0, L], \tag{6}$$

and the mixed Neumann–Dirichlet boundary conditions:

$$\frac{\partial c}{\partial x} = 0 \quad \text{as } t > 0, x = 0, \quad c = 0 \quad \text{as } t > 0, x = L, \tag{7}$$

which imply a no-flux condition at the GDL–CL interface, and zero concentration of dissolved ions at the CL–PEM interface.

Following [17], the reaction rates in (3)–(5) are given by the modified Butler–Volmer equations, which describe the Pt ion dissolution (1) by

$$r_{\text{dissol}}(c, d, \theta, V) = B_1(d, \theta) \exp\{(1 - \beta_1)B_4(d, \theta)V\} - cB_2(d, \theta) \exp\{-\beta_1 B_4(d, \theta)V\}, \tag{8}$$

in units of mol/(cm$^2 \times$s) and the Pt oxide coverage (2) by

$$r_{\text{oxide}}(\theta, V) = \Gamma \exp\left\{-\frac{1}{RT}(H_{2,\text{fit}} + \lambda\theta)\right\}\left(v_1^\star\left(1 - \frac{\theta}{2}\right)\exp\left\{-\frac{n_2 F(1 - \beta_2)}{RT}\left(U_{\text{fit}} + \frac{\omega\theta}{n_2 F}\right)\right.\right.$$
$$\left.\left. + (1 - \beta_2)\frac{n_2 F}{RT}V\right\} - v_2^\star 10^{-2pH}\exp\left\{\frac{n_2 F\beta_2}{RT}\left(U_{\text{fit}} + \frac{\omega\theta}{n_2 F}\right) - \beta_2\frac{n_2 F}{RT}V\right\}\right). \tag{9}$$

Equations (8) and (9) employ the auxiliary quantity B_1 (mol/(cm$^2 \times$s)):

$$B_1(d, \theta) = v_1 \Gamma(1 - \theta)\exp\left\{\frac{1}{RT}\left(-H_{1,\text{fit}} - nF(1 - \beta_1)\left(U_{\text{eq}} - \frac{4\Omega\gamma_0(\theta)}{nFd}\right)\right)\right\}, \tag{10}$$

the quantity B_2 (cm/s):

$$B_2(d, \theta) = \frac{v_2 \Gamma(1 - \theta)}{c_{\text{ref}}}\exp\left\{\frac{1}{RT}\left(-H_{1,\text{fit}} + nF\beta_1\left(U_{\text{eq}} - \frac{4\Omega\gamma_0(\theta)}{nFd}\right)\right)\right\}, \tag{11}$$

and the quantity B_4 (C/J):

$$B_4(d, \theta) = \frac{F}{RT}\left(n - \frac{4\Omega\Gamma n_2\theta}{d}\right), \tag{12}$$

where the expression of γ_0 (J/cm^2) is given by

$$\gamma_0(\theta) = \gamma + \Gamma RT\left(\theta\ln\left(\frac{v_2^\star}{v_1^\star}10^{-2pH}\right)\right.$$
$$\left. + \theta\frac{2n_2 FU_{\text{fit}} + \omega\theta}{2RT} + \theta\ln\left(\frac{\theta}{2}\right) + (2 - \theta)\ln\left(1 - \frac{\theta}{2}\right)\right). \tag{13}$$

All parameters employed in the system (3)–(13) are collected in Tables 1–3.

To numerically solve the system (3)–(7) with nonlinear reactions of the exponential type given by (8)–(13), we suggest a variable time-step 4th order Runge–Kutta method. For the square voltage profile, a step-size is refined locally at the electric potential lift-off from V_{min} to V_{max}. In the numerical tests, we set the coarse time step to $\tau_{\text{coarse}} = 10^{-2}$ s, and the uniform CL thickness spacing $h = L/10$ (cm). The fine time $\tau_{\text{fine}} = 10^{-4}$ s was sufficient inside $(-\tau_{\text{coarse}}, \tau_{\text{coarse}})$-neighborhood of the electric potential $V(t)$ lift-off from 0.6 to 0.9 (V) at the time $t_{\text{liftoff}} = 10$ s during each period, see Figure 1b.

3. Results

We calculate the relative Pt mass ratio with the help of the particle diameter d divided by the constant d_{Pt} from the initial condition in (6) at $t = 0$ as follows:

$$m_{Pt}(t, x) = \frac{4}{3} \pi \left(\frac{d(t,x)}{2} \right)^3 / V_{Pt} = \left(\frac{d(t,x)}{d_{Pt}} \right)^3 \quad \text{for } t \geq 0, \, x \in [0, L], \tag{14}$$

such that $m_{Pt} \in [0, 1]$ for decay. Ignoring stronger Pt mass loss near the membrane than at the GDL interface, we average this quantity over the CL thickness as

$$\overline{m}_{Pt}(t) = \operatorname*{mean}_{x \in [0, L]} \big(m_{Pt}(t, x) \big). \tag{15}$$

We investigated how different fitting parameters taken from [6,17,18,21] impact the platinum catalyst degradation within the model (3)–(13). We vary the bulk equilibrium voltage of Pt dissolution $U_{eq} \in \{1.118, 1.133, 1.15, 1.18\}$ (V) and oxide formation $U_{fit} \in \{0.8, 0.805, 0.81, 0.815\}$ (V), Pt dissolution activation enthalpy $H_{1,fit} \in \{3.9, 4, 4.79, 6.39\} \times 10^4$ (J/mol), reference ion concentration $c_{ref} \in \{0.2, 1, 2, 3\}$ (mol/cm^3), while the value $H_{2,fit}$ given in Table 3 was found unique. The corresponding lines of the averaged platinum mass ratio $\overline{m}_{Pt}(t)$ on 100 cycles during 1 h 6 min 4 s are depicted in Figure 2.

(**a**)   (**b**)   (**c**)
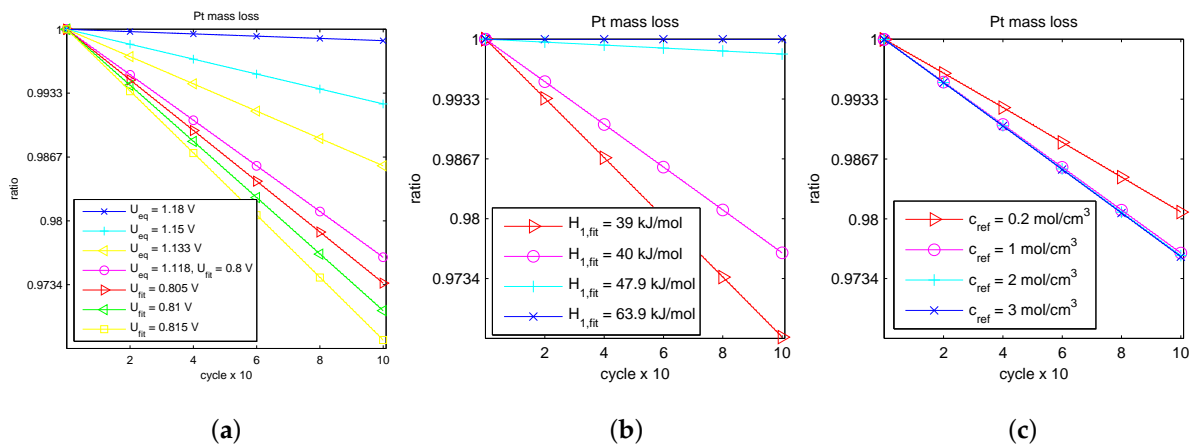
Figure 2. Pt loss when fitting: (**a**) Pt dissolution and oxide formation bulk equilibrium voltage; (**b**) Pt dissolution activation enthalpy; (**c**) reference ion concentration.

A decay in time of $\overline{m}_{Pt}$ affects the larger catalyst durability for smaller Pt mass loss rate, otherwise, drop for larger rate. Moreover, based on the linear decay seen in Figure 2, we calculated the slope $\overline{m}'_{Pt}$ and linearly extrapolated it with respect to a number of cycles up to $\overline{m}_{Pt} = 0$, when the catalyst is out of order. The lifetime prognosis is presented in Table 4 in descending order with respect to the predicted number of live cycles and hours of work. The reference parameter values are marked in color here.

In Table 4, we can observe essential differences in the lifetime prognosis when varying the fitting parameters.

Table 4. Lifetime when fitting: Pt dissolution and oxide formation bulk equilibrium voltage, Pt dissolution activation enthalpy, and reference ion concentration.

Symbol	Pt loss Rate$\times 10^{-6}$ (1/cycle)	Cycles Prognosis (#)	Work Prognosis (h)
$U_{eq} = 1.118$, $U_{fit} = 0.8$ (V), $H_{1,fit} = 4 \times 10^4$, $c_{ref} = 1$	237.89	4203	47
$U_{eq} = 1.18$ (V)	11.85	84,354	937
$U_{eq} = 1.15$ (V)	77.82	12,850	143
$U_{eq} = 1.133$ (V)	142.42	7021	78
$U_{fit} = 0.805$ (V)	264.84	3776	42
$U_{fit} = 0.81$ (V)	293.61	3405	38
$U_{fit} = 0.815$ (V)	324.27	3084	34
$H_{1,fit} = 6.39 \times 10^4$ (J/mol)	0.07	13,736,300	152,625
$H_{1,fit} = 4.79 \times 10^4$ (J/mol)	16.48	60,677	674
$H_{1,fit} = 3.9 \times 10^4$ (J/mol)	331.58	3015	34
$c_{ref} = 0.2$ (mol/cm^3)	192.29	5200	58
$c_{ref} = 2$ (mol/cm^3)	240.89	4151	46
$c_{ref} = 3$ (mol/cm^3)	241.98	4132	46

4. Discussion

We compare the relative impact of the parameters by measuring the output $\overline{m}'_{Pt}$ from variation of a specific input X with the help of PCC

$$\rho_X = \frac{\text{cov}(X, \overline{m}'_{Pt})}{\sqrt{\text{Var}(X)\text{Var}(\overline{m}'_{Pt})}} \in [-1, 1]. \qquad (16)$$

For the fitting parameters $X \in \{U_{eq}, U_{fit}, H_{1,fit}, c_{ref}\}$ from Table 4, respective Pearson coefficients ρ_X are gathered in ascending order in Table 5.

Table 5. Variance and correlation coefficients for input and output parameters.

Parameter	Var(X)	Var($\overline{m}'_{Pt}$)	ρ_X
$X = U_{eq}$	5.31×10^{-4}	6.96×10^{-9}	-0.96
$X = H_{1,fit}$	9.94×10^7	2.02×10^{-8}	-0.83
$X = c_{ref}$	1.11	4.33×10^{-10}	0.78
$X = U_{fit}$	3.12×10^{-5}	1.04×10^{-9}	0.99

The magnitude $|\rho_X|$ characterizes sensitivity of the model to variation of a specific parameter X. A positive sign $\rho_X > 0$ means that an increase of X increases the Pt mass loss and reduces lifetime. A negative sign $\rho_X < 0$ implies a decrease of the platinum loss and raises lifetime.

From Table 5, we conclude that the model is more sensitive to change of the Pt dissolution bulk equilibrium voltage U_{eq} and Pt oxide formation bulk equilibrium voltage U_{fit} and less sensitive when changing the Pt dissolution activation enthalpy $H_{1,fit}$ and reference Pt ion concentration c_{ref}, whereas a decrease of U_{eq}, $H_{1,fit}$ and an increase of U_{fit}, c_{ref} lengthen lifetime. These results are of interest for future studies to compare data of numerical simulations that can be found in the literature.

5. Conclusions

We presented the result of the variance-based sensitivity analysis for PEMFC cycling durability with respect to variation of the selected fitting parameters. Using regression analysis, we found that fitting parameters of Pt dissolution and oxide formation bulk equilibrium voltage have the highest tendency to degrade the PEM membrane for our modeling. Direct comparison of the numerical study with a real-time working model is

little-known because rare data of protocols and operating conditions are freely available in the literature. The more accurate conditions for the modeling of prolonged cycling durability by varying temperature, relative humidity, ionomer volume fraction in cathode, Pt particle size, loading, and diffusion coefficient characterizing the platinum ions transport is the subject of a forthcoming work.

Institutional Review Board Statement: Not applicable.

Informed Consent Statement: Not applicable.

Data Availability Statement: Not applicable.

Conflicts of Interest: The author declares no conflict of interest.

Abbreviations

The following abbreviations are used in this manuscript:

AST	accelerated stress test
C	carbon
CL	catalyst layer
FC	fuel cell
GDL	gas diffusion layer
PCC	Pearson correlation coefficient
Pt	platinum
PtO	platinum oxide
Pt^{2+}	platinum ion
PEM	polymer electrolyte membrane

References

1. Eikerling, M.; Kulikovsky, A. *Polymer Electrolyte Fuel Cells: Physical Principles of Materials and Operation*; Elsevier: Amsterdam, The Netherlands, 2017.
2. Hacker, V.; Mitsushima, S. (Eds.) *Fuel Cells and Hydrogen: From Fundamentals to Applied Research*; Elsevier: Amsterdam, The Netherlands, 2018.
3. Kulikovsky, A.; Berg, T. Positioning of a reference electrode in a PEM fuel cell. *J. Electrochem. Soc.* **2011**, *162*, F843–F848. [CrossRef]
4. Karpenko-Jereb, L.; Araki, T. Modeling of polymer electrolyte fuel cells. In *Fuel Cells and Hydrogen: From Fundamentals to Applied Research*; Hacker, V., Mitsushima, S., Eds.; Elsevier: Amsterdam, The Netherlands, 2018; pp. 41–62.
5. Karpenko-Jereb, L.; Sternig, C.; Fink, C.; Tatschl, R. Membrane degradation model for 3D CFD analysis of fuel cell performance as a function of time. *Int. J. Hydrogen Energy* **2016**, *41*, 13644–13656. [CrossRef]
6. Pandy, A.; Yang, Z.; Gummalla, M.; Atrazhev, V.V.; Kuzminyh, N.Y.; Sultanov, V.I.; Burlatsky, S. A carbon corrosion model to evaluate the effect of steady state and transient operation of a polymer electrolyte membrane fuel cell. *J. Electrochem. Soc.* **2013**, *160*, F972–F979. [CrossRef]
7. Fellner, K.; Kovtunenko, V.A. A singularly perturbed nonlinear Poisson–Boltzmann equation: Uniform and super-asymptotic expansions. *Math. Meth. Appl. Sci.* **2015**, *38*, 3575–3586. [CrossRef]
8. Fellner, K.; Kovtunenko, V.A. A discontinuous Poisson–Boltzmann equation with interfacial transfer: Homogenisation and residual error estimate. *Appl. Anal.* **2016**, *95*, 2661–2682. [CrossRef]
9. González Granada, J.R.; Kovtunenko, V.A. Entropy method for generalized Poisson–Nernst–Planck equations. *Anal. Math. Phys.* **2018**, *8*, 603–619. [CrossRef]
10. Dreyer, W.; Guhlke, C.; Müller, R. A new perspective on the electron transfer: Recovering the Butler–Volmer equation in non-equilibrium thermodynamics. *Phys. Chem. Chem. Phys.* **2016**, *18*, 24966–24983. [CrossRef]
11. Kovtunenko, V.A.; Reichelt, S.; Zubkova, A.V. Corrector estimates in homogenization of a nonlinear transmission problem for diffusion equations in connected domains. *Math. Meth. Appl. Sci.* **2020**, *43*, 1838–1856. [CrossRef]
12. Kovtunenko, V.A.; Zubkova, A.V. On generalized Poisson–Nernst–Planck equations with inhomogeneous boundary conditions: a-priori estimates and stability. *Math. Meth. Appl. Sci.* **2017**, *40*, 2284–2299. [CrossRef]
13. Kovtunenko, V.A.; Zubkova, A.V. Mathematical modeling of a discontinuous solution of the generalized Poisson–Nernst–Planck problem in a two-phase medium. *Kinet. Relat. Mod.* **2018**, *11*, 119–135. [CrossRef]
14. Kovtunenko, V.A.; Zubkova, A.V. Homogenization of the generalized Poisson–Nernst–Planck problem in a two-phase medium: correctors and estimates. *Appl. Anal.* **2021**, *100*, 253–274. [CrossRef]

15. Kovtunenko, V.A.; Zubkova, A.V. Existence and two-scale convergence of the generalised Poisson–Nernst–Planck problem with non-linear interface conditions. *Eur. J. Appl. Math.* **2021**, *32*, 683–710. [CrossRef]

16. Khludnev, A.M.; Kovtunenko, V.A. *Analysis of Cracks in Solids*; WIT-Press: Boston, MA, USA, 2000.

17. Holby, E.F.; Morgan, D. Application of Pt nanoparticle dissolution and oxidation modeling to understanding degradation in PEM fuel cells. *J. Electrochem. Soc.* **2012**, *159*, B578–B591. [CrossRef]

18. Li, Y.; Moriyama, K.; Gu, W.; Arisetty, S.; Wang, C.Y. A one-dimensional Pt degradation model for polymer electrolyte fuel cells. *J. Electrochem. Soc.* **2015**, *162*, F834–F842. [CrossRef]

19. Kannan, R.; Kim, A.R.; Kim, J.S.; Yoo, D.J. 3D graphene-mixed metal oxide-supported carbonsingle bondpalladium quantum dot nanoarchitectures—A facile bifunctional electrocatalyst for direct ethylene glycol fuel cells and oxygen evolution reactions. *Int. J. Hydrogen Energy* **2016**, *41*, 18033–18043. [CrossRef]

20. Kumar, T.R.; Yoo, D.J.; Kim, A.R.; Kumar, G.G. Green synthesis of Pt–Pd bimetallic nanoparticle decorated reduced graphene oxide and its robust catalytic activity for efficient ethylene glycol electrooxidation. *New J. Chem.* **2018**, *42*, 14386–14393. [CrossRef]

21. Kovtunenko, V.A.; Karpenko-Jereb, L. Study of voltage cycling conditions on Pt oxidation and dissolution in polymer electrolyte fuel cells. *J. Power Source* **2021**, *493*, 229693. [CrossRef]

22. Kovtunenko, V.A.; Karpenko-Jereb, L. Lifetime of catalyst under voltage cycling in polymer electrolyte fuel cell due to platinum oxidation and dissolution. *Technologies* **2021**, *9*, 80. [CrossRef]

23. Pivac, I.; Barbir, F. Impact of shutdown procedures on recovery phenomena of proton exchange membrane fuel cells. *Fuel Cells* **2020**, *160*, 185–195. [CrossRef]

24. Jayakumar, A.; Madheswaran, D.K.; Kumar, N.M. A critical assessment on functional attributes and degradation mechanism of membrane electrode assembly components in direct methanol fuel cells. *Sustainability* **2021**, *13*, 13938. [CrossRef]

25. Wang, X.Z.; Zhang, M.M.; Shi, D.D.; Zhang, S.C.; Wu, Y.M.; Gong, W.J.; Fan, H.Q. Long-term polarization accelerated degradation of nano-thin C/Ti coated SS316L bipolar plates used in polymer electrolyte membrane fuel cells. *Int. J. Hydrogen Energy* **2022**, *47*, 8974–8992. [CrossRef]

26. Testa, E.; Maggiore, P.; Pace, L.; Dalla Vedova, M.D.L. Sensitivity analysis for a PEM fuel cell model aimed to optimization. *WSEAS Trans. Power Syst.* **2015**, *10*, 171–179.